

Smart Switch Metamaterials for Multiband Radio Frequency Antennas

PAUL J. WOLCOTT,¹ CHRISTOPHER D. HOPKINS,¹ LANLIN ZHANG² AND MARCELO J. DAPINO^{1,*}

¹*Smart Materials and Structures Laboratory, Department of Mechanical and Aerospace Engineering, The Ohio State University, Columbus, OH 43210, USA*

²*ElectroScience Laboratory, Department of Electrical and Computer Engineering, The Ohio State University, Columbus, OH 43210, USA*

ABSTRACT: We investigate metal–matrix composite metamaterials with embedded electrical switches made of shape memory nickel–titanium (Ni–Ti) for use in broadband radio frequency (RF) antennas. Experiments show that a Ni–Ti ribbon can form an electrical contact that opens and closes depending on the Ni–Ti phase being austenite or martensite. Finite element modeling of thermal gradients illustrates the phase change within the ribbon. Ultrasonic additive manufacturing (UAM), a solid-state additive manufacturing process, was utilized for embedding a Ni–Ti switch in an aluminum matrix. The aluminum matrix must have structural-grade strength for use in load-carrying antennas; thus, mechanical testing was conducted to quantify the longitudinal tensile, transverse tensile, and shear strength of the UAM matrix. Reconfiguration using a Ni–Ti switch was proven using a shape memory switch on a monopole RF antenna producing an operating frequency shift from 270 to 185 MHz when the switch is connected. A planar microstrip line was used to demonstrate signal transmission and reflection efficiency in a smaller, second switch. Transmission tests yielded less than –10 dB signal reflection proving the feasibility of reconfigurable planar antenna arrays using smart switches.

Key Words: ultrasonic additive manufacturing, ultrasonic consolidation, metamaterials, metal matrix composites, smart materials, RF antennas.

INTRODUCTION

METAMATERIALS are synthetic, three-dimensional periodic cellular architectures designed to exhibit optimized responses. Recently, metamaterials have been considered for radio frequency (RF) and optical applications. The intrinsically narrowband behavior of these materials, however, has limited their use to narrowband ground planes emulating magnetic layers or creating thinner conformal antennas (Volakis et al., 2006; Ziolkowski, 2008; Caloz, 2009).

The objective of this research is to develop an approach to overcome the narrowband limitation of metamaterials and realize multiband/broadband structural antennas with potential frequency bandwidth of 30:1 (100–3000 MHz). Reconfiguration through changes in antenna geometry is one method of creating wide frequency bandwidth for antenna applications. Smart materials can enable antenna reconfiguration through mechanical and

electromechanical tuning. Specific applications include the ability to achieve miniature conformal ultra wideband antennas (30–3000 MHz) on thin and flexible substrates for small Unmanned Aerial Vehicles (UAVs), high gain antennas for portable devices enabling high-data rate communications *via* ground and satellite means, and multifunctional and reconfigurable apertures.

To create a wide bandwidth reconfigurable antenna, changes in geometry or material properties of the antenna must be realized. Changes in geometry require additions or subtractions to the electrical signal pathway of the antenna to create a different working frequency. Previous approaches to geometric reconfiguration, such as MEMS devices, provide a small change in geometry due to their size. Therefore, it has been difficult to produce changes on a large range of frequencies (Yashchyshyn, 2010). Reconfiguration through changes in material properties such as electrical permittivity requires a solid-state change of the electrical properties of the antenna materials to change the resonance frequency of the antenna. Approaches such as using silicon require activation *via* optical light, making it more difficult to incorporate these approaches into a load-

*Author to whom correspondence should be addressed.
Email: dapino.1@osu.edu
Figures 2 and 4–17 appear in color online: <http://jim.sagepub.com>

bearing design (Yashchyshyn, 2010). Shape memory alloys (SMAs) can operate over a large range of geometric dimensions and only require heating elements (often electrical resistive heating) for actuation allowing them to achieve resonance frequency shifting within a load-bearing, enclosed structure.

This study investigates the design and fabrication of metal–matrix composites with embedded reconfiguration based on smart materials such as Ni–Ti SMAs. These alloys can plastically deform and then recover their original shape when the temperature is increased above their austenitic finish temperature. Ni–Ti is a specific type of SMA able to withstand strain up to 8% and fully recover all deformation (Lagoudas, 2008). The large recoverable strain is due to the crystal-line structure of the alloy transforming between martensite and austenite (Lagoudas, 2008). The martensite phase has two monoclinic microstructures, twinned and detwinned. The twinned form consists of alternating monoclinic orientations that, upon application of stress, are reorganized in the same direction forming the detwinned phase. The austenitic phase is a cubic crystalline microstructure that is recovered upon heating martensite. After cooling of the austenitic phase with no stress applied, the alloy transforms back into the twinned martensitic microstructure. The design investigated here uses the unique characteristics of Ni–Ti in a solid-state actuator to open and close a simple electrical switch. Two switches are designed and fabricated based on these principles.

Embedding smart materials in a metal–matrix forms the building block for a metamaterial with load-bearing properties. The manufacturing process used to embed smart materials into metal matrices is ultrasonic additive manufacturing (UAM), also known as ultrasonic consolidation. UAM is a recent manufacturing process which combines principles of ultrasonic metal welding, layered manufacturing techniques, and subtractive processes for creation of metal parts with arbitrary shapes and features (Graff, 2005). The UAM process is a solid-state welding process joining metallic materials well below their respective melting temperatures. The ultrasonic vibration generates local heating in the range of 30–50% of the melting temperature of the base metal (Kong et al., 2004). Due to the low temperatures generated in the UAM process, UAM offers unprecedented opportunities to create parts with embedded smart materials or electronic components (Kong and Soar, 2005; Siggard, 2007). Also, a subtractive stage integrated within the UAM system allows the simultaneous incorporation of arbitrarily shaped internal features such as channels or designed anisotropies. Aluminum 3003 has been used frequently in the UAM process because of its usefulness as a lightweight alloy and the relative ease with which it can be welded through UAM.

DEVELOPMENT OF SMA SWITCH

Geometry and Proof of Concept

To simplify the switch mechanism while still performing the required action, several switch configurations were considered. The main constraints and considerations surrounding the creation of the switch include the size of the gap needed to prevent electrical arcing at the switch contact point, the geometry and material needed to close and open the switch, and the method and material for joining parts of the switch. Study of various geometries and materials showed that a normally-open switch could be most easily configured, tested, and embedded by UAM into a metal matrix. A bilayer of 7.62 mm wide by 0.254 mm thick Ni–Ti strip and 12.7 mm wide by 0.102 mm thick spring steel was found to work best in switch 1. The Ni–Ti transformation temperatures as measured with differential scanning calorimetry are $A_s = 58^\circ\text{C}$, $A_f = 71^\circ\text{C}$, $M_s = 51^\circ\text{C}$, and $M_f = 42^\circ\text{C}$. Epoxy was used to adhere the Ni–Ti ribbon to the spring steel. The configuration of steel and Ni–Ti is shown in Figure 1.

The Ni–Ti ribbon, in this configuration, pushes down on the spring steel during the phase transformation from martensite to austenite thus restoring the flat memorized shape. After heating concludes, the Ni–Ti ribbon plastically deforms back up due to the elasticity of the spring steel. Assisted by the kinematic gain created by the bump in the Ni–Ti ribbon, the total travel of the switch was initially 1.905 cm, later reduced to 0.50 cm by adjusting the memorized shape of the Ni–Ti ribbon. Shorter travel distance leads to shorter switching time and reduced overall size, which is beneficial for embedment. Since the strains involved with the actuation are on the order of 1%, degradation of the shape memory effect is limited as detailed in Huang (2002).

Electrical Insulation

Electrically insulating the Ni–Ti ribbon and spring steel bilayers from the surrounding metal matrix and from each other is critical to the operation of the switch. Insulation ensures that electrical contact is achieved only when the shape memory ribbon is actuated to the fully closed position without short circuits



Figure 1. Normally-open Ni–Ti and steel switch configuration and geometry.

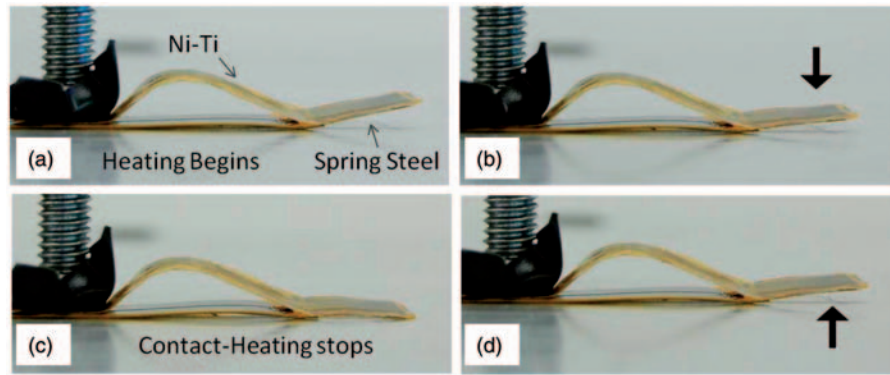


Figure 2. Images of SMA switch 1 where (a) switch is in initial position; (b) heating has begun and switch begins to close; (c) switch has fully closed and is in contact with metal below; (d) cooling has begun and switch returns to original position due to spring steel.

due to the heating elements. The insulation needs to be joined directly to the Ni–Ti ribbon for complete electrical separation. Further, it is necessary that the insulation layer be as thin as possible to avoid disrupting the embedding process. Finally, the insulation must be tough enough to withstand the high oscillatory shear forces present during the UAM process.

Investigations were conducted using several different methods and materials for electrical insulation. Two insulation coatings studied include Epoxylite insul-spray clear enamel, and a polyimide based insulating varnish. It was found that while both coatings are able to fully encapsulate and insulate the Ni–Ti ribbon, neither can withstand the embedding process. Post-embedding tests found that there was electrical conductivity between the Ni–Ti ribbon and the surrounding aluminum matrix confirming that the insulation is compromised during UAM. A Teflon coating was applied to the Ni–Ti ribbon, but the layer applied was not thick enough to fully insulate the strip and further investigations were not pursued. Anodizing the Ni–Ti ribbon to create a thick oxide layer on the surface of the strip was considered; however, numerous attempts were unsuccessful at producing a thick enough layer to fully encapsulate the Ni–Ti strip. Kapton film was shown to be an effective insulator. It electrically insulates the steel and Ni–Ti ribbon, and is thin enough (0.127 mm) to facilitate embedding. In addition, Kapton was shown to withstand the oscillating shear forces created during the UAM process.

Switch Design and Finite Element Modeling

The switch actuation cycle with an externally applied heat source is shown in Figure 2. These images demonstrate the operation of the switch as described in the Geometry and Proof of Concept section. The Ni–Ti ribbon was machined *via* electron discharge machining (EDM) to create a small gap in the strip through part of its length, as shown in Figure 3. This gap creates an electric circuit such that current passed through the

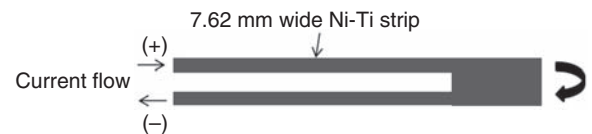


Figure 3. Schematic of Ni–Ti strip circuit used for resistive heating of smart switch 1.

Ni–Ti ribbon creates ohmic heating and an associated solid state phase transformation.

The test setup thus consists of a high current circuit for heating of the Ni–Ti ribbon and a low-current switchable circuit that creates the test signal. Figure 4 shows the setup used for testing the switch. The Ni–Ti ribbon and most of the spring steel are fully encapsulated in Kapton film. A small portion of the spring steel at the tip was left un-insulated to allow current to run through the switch to the metal matrix surrounding it. Behind the bump portion of the Ni–Ti ribbon, the bilayer was mechanically clamped to prevent the Ni–Ti ribbon from actuating in the wrong direction and to simulate the conditions that would occur when embedded.

In the test setup, one power supply produces a DC current of about 5 A directed through the Ni–Ti strip circuit to resistively heat the Ni–Ti ribbon. The second power supply is used to create a test signal with approximately 0.75 A of current. When the switch is open, no current flows through the steel and aluminum matrix circuit. When the switch is fully closed, current flows through the steel (at the exposed end) into the aluminum baseplate and back to the power supply as the test signal. During testing, the currents were measured simultaneously and the resulting current vs time plot is shown in Figure 5.

Figure 5 shows the current ramping to the desired value of about 5 A and holding while the Ni–Ti austenitic phase transformation temperature is reached and the switch begins to actuate (0–17 s). The switch is then fully closed and the test signal (blue-dashed line) steps up to a current of about 0.75 A and holds (17–27 s). The current

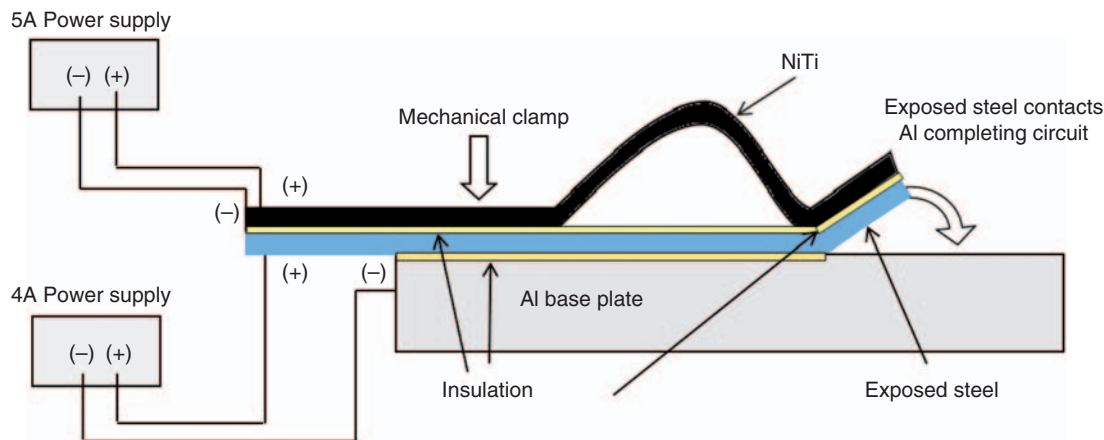


Figure 4. Diagram of setup used for testing SMA switch 1.

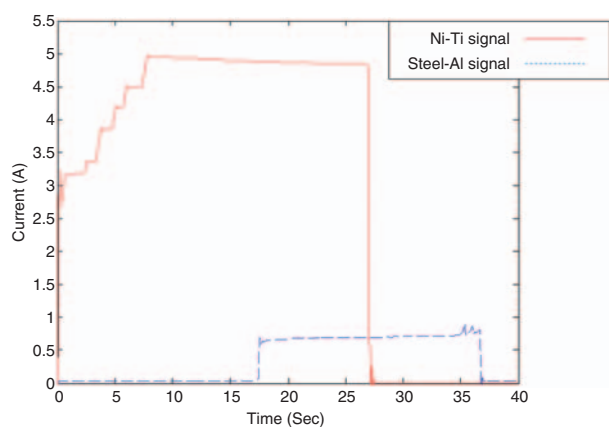


Figure 5. Plot of current vs time showing the closing of SMA switch 1, resulting current through the Al-steel circuit, opening of the SMA switch and time delayed response of opening of Al-steel circuit.

through the Ni–Ti element is then shut-off and the switch begins to cool, transforming the Ni–Ti into martensite, deforming due to the spring steel and breaking contact cutting the test signal (27–36 s). This test proves that the switch works correctly. The actuation speed can be optimized depending upon the current applied through the Ni–Ti element, the distance that the switch needs to travel in order to make contact, and the cooling conditions. The actuation speed does not have any effect on the frequency that the switch operates, only on the time to reconfigure between geometries.

Finite element analysis using Comsol Multiphysics 3.5a was performed on the Ni–Ti switch geometry to simulate heating and cooling cycles during operation. A Ni–Ti ribbon with a 4.06 cm mechanically free section (actuating portion) and a 16.26 cm section encapsulated in an aluminum matrix, was modeled. A 4.95 A current was modeled to heat the wire by current conduction through the right side of the split end of the Ni–Ti switch with the left side of the split end grounded. The model uses passive heating as a means to describe the

heat distribution created by the resistive heating as current is passed through. Phase transformation-related latent heat was not included in the modeling. From the equations related to latent heat phase transformations given by Waram (1993), latent heat effects could contribute up to an approximately 50% increase in the time for transformation when heating. The purpose of our modeling is to ascertain the heat distribution in the Ni–Ti switch in steady-state, which is not greatly affected by the heating time constant. Therefore, the latent heat was not considered in this model.

Finite element analysis of the Ni–Ti model shows that the section of Ni–Ti encapsulated in the aluminum matrix rises only 1°C while the mechanically free section of the Ni–Ti ribbon increases to much higher temperatures (Figure 6). Temperature as a function of time plots for the three main sections examined are shown in Figure 7. The split portion of the mechanically free section of the Ni–Ti actuator increases to a peak temperature of 70°C at the applied current. The mechanically-free large cross-section at the tip experiences lower temperatures than the split portion of the Ni–Ti ribbon. This is due to lower electrical power created because the larger cross-sectional area causes less current flow due to its greater impedance. The variation in temperature in the actuating region indicates that during resistive heating, only the split portion in the actuation region transforms to austenite. The larger tip region remains in the martensite phase during the entire thermal cycle and serves only as a physical connection between the cantilever spring and the switch. Thus, the Ni–Ti geometry used maximizes the efficiency of the switch by only using enough current to sufficiently heat the small section that applies the force (split section), while not wasting current on sections that do not contribute to the actuation. The cooling cycle of the Ni–Ti switch occurs relatively quickly due to the aluminum matrix conducting heat out of the Ni–Ti ribbon more rapidly than if the ribbon were in ambient air, as shown in Figure 8.

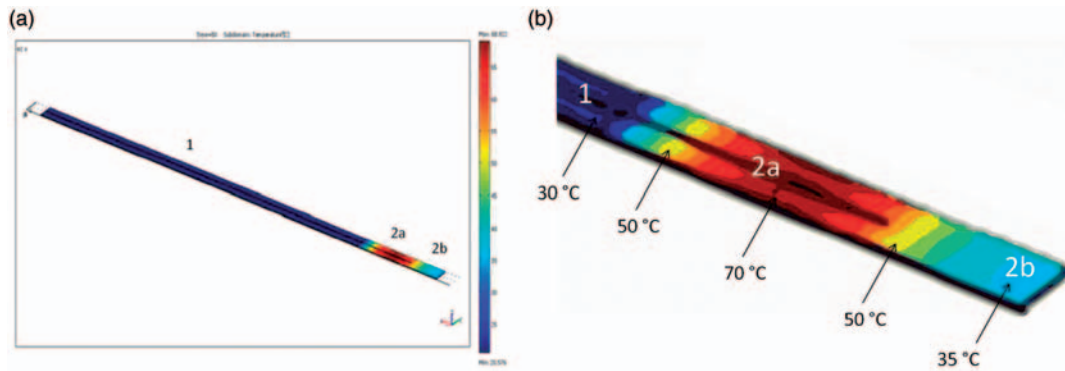


Figure 6. (a) Modeled temperature profile of Ni–Ti switch 1 after 50 s heating where region 1 is Ni–Ti in Al matrix; region 2 is the mechanically free segment, region 2a is the actuating split section, and region 2b is the tip contact area. (b) Zoomed-in representation of the temperature distribution around the actuating region.

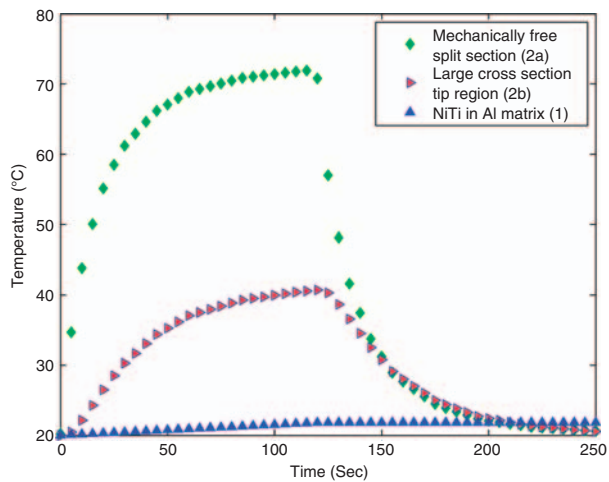


Figure 7. Temperature vs time plot of different sections of Ni–Ti switch 1.

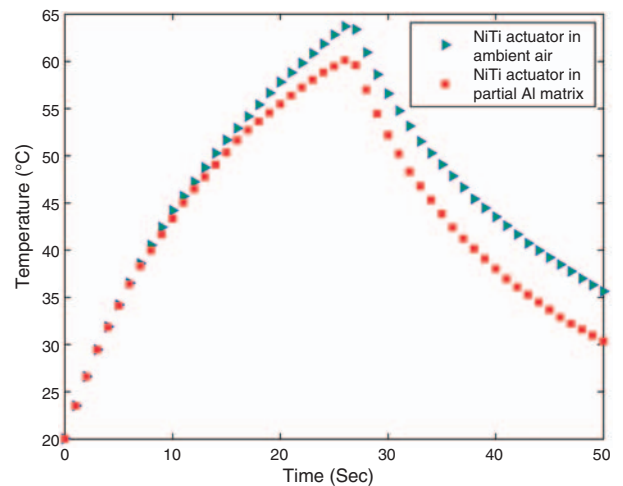


Figure 8. Temperature vs time plot of Ni–Ti switch 1 in ambient air compared to Ni–Ti partially embedded in Al matrix.

An infrared image of a sample switch was taken as a comparison to the model, similar to Huang et al. (2004). As seen in Figure 9, the distribution of heat from the image is similar to the FEA model, with a few differences. The figure shows greater heating in the right side of the split portion of the Ni–Ti than the left. This is due to the right side having a smaller width than the left side due to uneven sectioning. Also there are other minor differences in the measured temperatures compared to the model due to measurement variability in the IR system. Overall, the measured distribution compares favorably to the model.

UAM COMPOSITES AND SWITCH INTEGRATION

Mechanical Characterization of UAM Matrix

The mechanical properties of UAM-fabricated parts govern the range of applications for which the process

may be used. Three distinct UAM samples were made to test the strength of the UAM matrix in shear, transverse tensile, and longitudinal tensile loading conditions. The averaged results of the mechanical tests are shown in Table 1. It has been found that shear and transverse tensile samples fail in a sudden, macro-brittle fracture mode with strengths less than the parent material. Longitudinal tensile samples exhibit ductile failure with an increase in strength over the parent material. It has been suggested that the increased strength is due to grain refinement from the horn texture and ultrasonic vibration (Johnson, 2008). It has also been found that the strength of the UAM builds is significantly influenced by the machine setting conditions and much research has been devoted to determining the optimal levels of the process parameters in order to maximize the mechanical strength of UAM specimens in a variety of materials (Kong et al., 2004; Janaki Ram et al., 2006; Kulakov and Rack, 2009; Hopkins et al., 2010). Overall, the results of these mechanical tests indicate that

orientation of UAM structures relative to loading conditions is critical.

Embedding of Switch into UAM Matrix

The switch was successfully embedded into a 3003 H-18 aluminum matrix using Edison Welding Institute's (EWI) VHP-UAM Test Bed with a 4450 N normal force, 31.2 μm oscillation amplitude, and 25.4 mm/s weld rate. The switch is flipped over such that it closes upward making contact with the aluminum tape above it. It has been previously shown that designed internal features can be machined during the build process in the UAM Formation system (White, 2003). For simplicity, the pocket and groove were machined out of solid 3003 aluminum and four layers were laid over top by UAM. Figure 10 shows a three-dimensional CAD model of the switch and matrix geometry used for embedding and the actual piece prior to embedment. Figure 11 shows the embedded switch. Successful embedding proves the switch geometry is embeddable using UAM. Being a low temperature process, embedding the smart switches

via UAM is not expected to significantly affect the properties of the switches. In addition, the actuating portion of the switch is placed in a cavity which further reduces the localized heating the Ni–Ti ribbon experiences during the process.

RF STUDY SWITCH 1

Experimental Setup

A simple quarter wavelength monopole antenna was designed and fabricated to evaluate the effect of the Ni–Ti switch on antenna performance. As shown in Figure 12, the aluminum monopole is 25.4 cm tall and 0.457 cm in diameter, centered on a 81.28 cm diameter aluminum ground plane. These dimensions are chosen for antenna operation at and around 300 MHz (Kraus and Marhefka, 2003). In this setup, the switch was located close to the monopole and supported by Styrofoam (the foam does not interfere with the electromagnetic signals or the antenna performance). The split end of the switch was connected to a DC power supply (Agilent E3631A). Two ferrite chokes were used on the connecting wires to isolate the RF signals from the DC current because the wires and connections are within the near-field region (approximately 1 m radius) for this particular setup and thus can become coupled to the antenna system. When no current is applied ('switch off'), there is no contact between the monopole and the switch. When the current is applied ('switch on'), the switch bends and makes contact with the top of the monopole. The antenna has a straight monopole in the 'switch off' state, and a reconfigured bent monopole in the 'switch on' state. The RF signals were delivered from the bottom of the monopole and the reflection coefficient was measured by a network analyzer (Agilent N5242A, PNA-X) as it swept through a range of frequencies. The reflection coefficient is a dB scaling of the antenna parameter, reflection coefficient S_{11} , which is given by (Pojar, 2008)

$$S_{11} = \frac{V_r}{V_i} \quad (1)$$

where V_r and V_i are the reflected and incident voltages, respectively. The reflection coefficient as measured by the network analyzer is given by (Pojar, 2008)

$$RL = 20 \log S_{11} \quad (2)$$

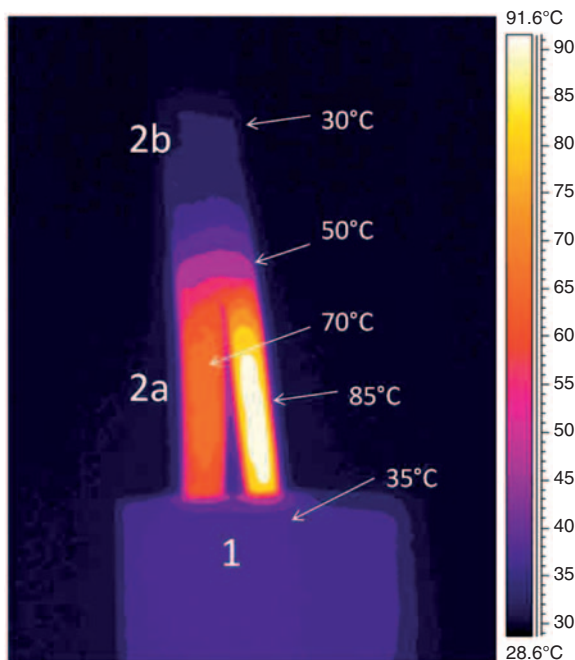


Figure 9. Infrared image of sample switch showing temperature distribution.

Table 1. Results of UAM mechanical strength tests and comparison to bulk 3003 H-18 aluminum.

Mechanical strength	Al 3003 H-18 (MPa) (The Aluminum Association, 1979)	UAM sample (MPa)	Percent of parent material (%)	Coefficient of variance (%)
Ultimate shear	110	53	47.8	16.6
Ultimate transverse tensile	200	30	15.2	9.45
Ultimate longitudinal tensile	200	236	117.8	2.46

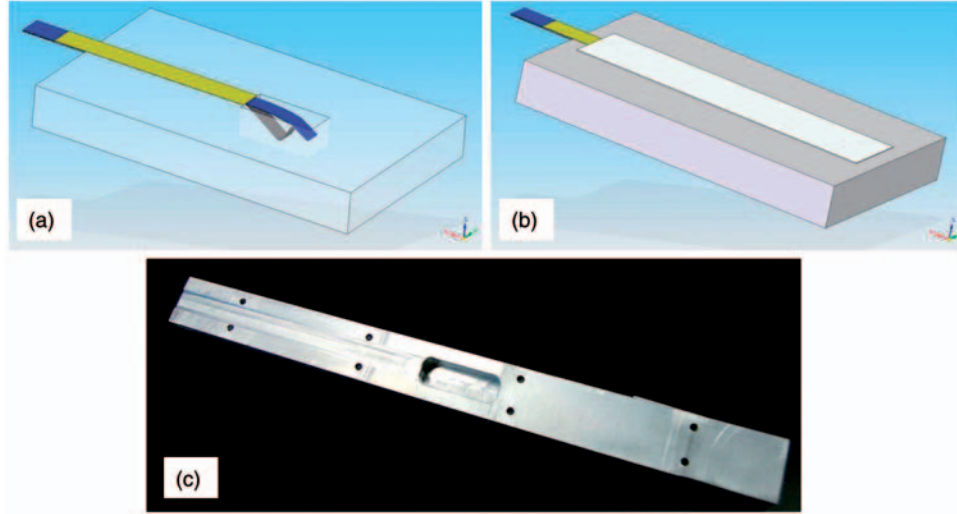


Figure 10. 3D CAD model of (a) Ni–Ti (black) and spring steel (blue) wrapped in Kapton (gold) in configuration to be embedded, (b) resulting embedded switch with aluminum layer (white) on top, and (c) photograph of machined aluminum piece prior to insertion of switch and embedding.

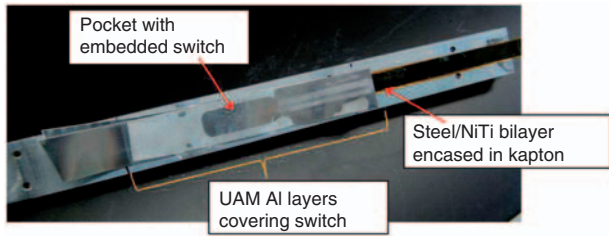


Figure 11. Image of UAM embedded Ni–Ti switch.

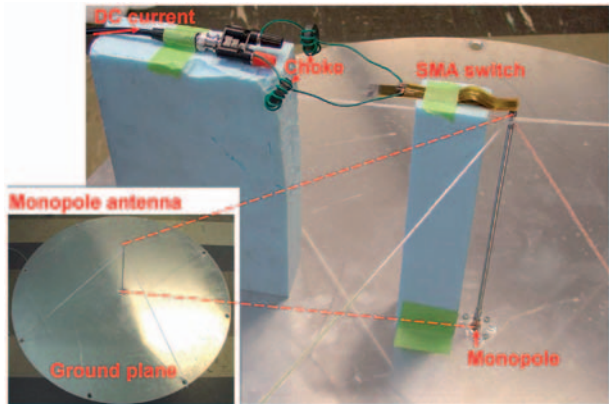


Figure 12. Images of monopole antenna and SMA switch setup for RF performance testing of switch 1.

This can also be written in terms of a power ratio such that $(V_r/V_i)^2 = (P_r/P_i)$ where P_r and P_i are the reflected and incident powers, respectively. In this case, the reflection coefficient is

$$RL = 10 \log \frac{P_r}{P_i} \quad (3)$$

Since S_{11} is determined by the antenna geometry and related impedance, it is useful for evaluating the performance changes at the different on and off switch states. The greater the negativity of S_{11} (in dB) the less signal is reflected back, thereby increasing the signal transmitted and leading to better RF performance.

Results

As depicted in Figure 13, the minimum S_{11} is -15.1 dB at 270 MHz with the switch off. When energized, the switch gradually bends toward the monopole, while the resonance frequency accordingly shifts to a lower frequency. Once the switch is in contact with the monopole, S_{11} is -14.5 dB at 185 MHz. The downward shift of the resonance peak is due to the extended length of the monopole in the ‘switch on’ state. It is also noted that S_{11} is less than -10 dB in both of the ‘off’ and ‘on’ states. This indicates that the reflected power is less than 10%, which is satisfactory for a working antenna. Therefore, this measurement shows that the antenna reconfiguration providing a shift in the working frequency can be achieved by incorporation of the Ni–Ti switch.

RF STUDY SWITCH 2

Switch Design

Using the principles discovered in the initial design and development of SMA switch 1, a second, smaller switch was developed. This was necessary to improve the feasibility of embedding as well as to provide greater flexibility in the design of a future switch array. The second switch consists of a bilayer of 3 mm wide by 0.254 mm thick Ni–Ti strip and 3.5 mm wide by

0.102 mm thick spring steel. This configuration works similarly to switch 1 where the heated Ni–Ti ribbon presses on the spring steel as it restores to its flat memorized shape during the transition from martensite to austenite. As heating is stopped, the elasticity of the spring steel deforms the Ni–Ti back up similarly as before. The travel distance of the switch was further decreased to 0.40 cm to reduce switching time and overall size. A comparison of the two switch designs can be seen in Figure 14. Switch 2 used Kapton film to insulate the Ni–Ti element from the spring steel similarly to switch 1.

To verify the operation of the second switch, a switch current test was conducted similar to that of switch 1. In this case, a DC current of about 3.4 A was applied *via* a power supply to the Ni–Ti to resistively heat and actuate the switch. Figure 15 shows the results of the currents vs. time. The results indicate that switch 2 actuation occurs more quickly and at a lower operating current than switch 1, both desired effects of the smaller dimensions.

Microstrip Line Construction

Due to its smaller dimensions, the second SMA switch is more suitable for planar antennas and electronic devices. To prove this concept, a simple microstrip transmission line (MTL) geometry was constructed and tested. A reference MTL sample was assembled consisting of a copper line 2.38 mm wide by 50 mm long on

a dielectric substrate (Rogers 6010LM, dielectric constant $\epsilon_r = 10.2$, dielectric loss $\tan \delta = 0.0023$) with a copper ground plane. The line dimensions were chosen such that the resultant impedance was 50Ω , matching the coaxial cables used in the network analyzer. The working microstrip transmission line sample was fabricated similarly, except for a 2.0 mm gap at the center of the line, as shown in Figure 16. The switch was located perpendicular to the gap and controlled by a direct current power supply as shown in Figure 16(b). The connecting DC wires were shielded from RF signals using two ferrite chokes. When no current was applied ('switch off'), there was no contact between the switch and the microstrip transmission line. When direct current was applied ('switch on'), the switch actuated downward to reconnect the microstrip transmission line between the gap in the copper. The working MTL thus only transmitted signals in the 'on' state. The reference microstrip transmission line sample was used to validate the performance of the working MTL when turned 'on'. The forward transmission coefficient (S_{21}) and reflection

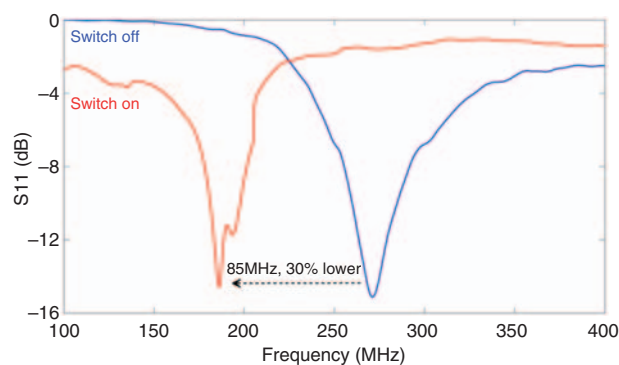


Figure 13. Reflection coefficient as a function of frequency for switch off and switch on states for switch 1.



Figure 14. Comparison of switch 1 and switch 2 sizes.

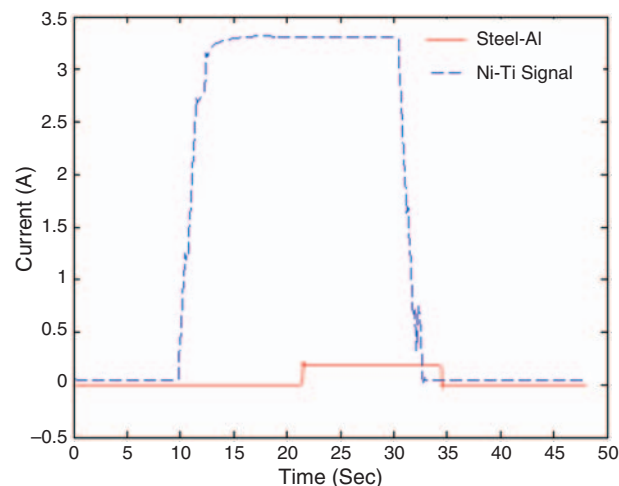


Figure 15. Switch 2 current test showing opening and closing of the switch.

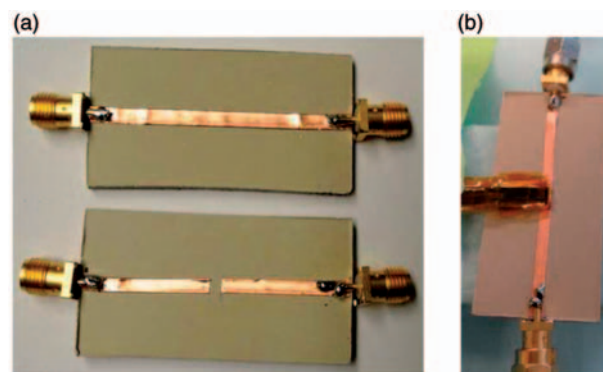


Figure 16. (a) Reference (upper) and working (lower) MTL samples (b) working MTL with SMA switch 2 connected.

coefficient (S_{11}) were measured by a network analyzer (Agilent N5242A, PNA-X) through a range of frequencies.

Microstrip Transmission Tests Using Switch 2

As depicted in Figure 17, when the working MTL is ‘Off’ the S_{11} is close to 0 dB indicating that nearly the entire signal is reflected back. When the working MTL is ‘On’, S_{11} less than -20 dB is achieved, showing most of the signal transmitted through. Compared with the reference MTL, the S_{21} is slightly lower due to imperfect contact between the switch and MTL. Nonetheless, the SMA switch proved successful in applications of a working MTL structure. This serves as a starting point for designing reconfigurable planar antennas with more complex geometries and circuits.

CONCLUSIONS AND FUTURE WORK

The initial steps toward creating a structural antenna made of a metal–matrix composite metamaterial with broadband reconfiguration were completed. A proof-of-concept smart material (Ni–Ti) switch was successfully created. Kapton film was found to be a robust electrical insulator able to withstand the high shear forces of UAM embedding. An experiment was devised and carried out testing the actuation properties of the switch. It was

found that a steady test signal can be applied through the spring steel and aluminum matrix by running a separate high current through the Ni–Ti ribbon to resistively heat the switch and create the desired actuation. Finite element modeling and infrared imaging showed that only the small region that provides the actuation is heated. Mechanical tests including transverse shear, transverse tensile, and longitudinal tensile conducted on 3003 aluminum UAM built samples showed that the orientation of the structure relative to the loading conditions is critical. RF performance tests using a simple monopole antenna and ground plane prove that a shift in resonant frequency of the antenna system is achievable through the actuation of an SMA switch. Microstrip line tests of a planar arrangement proved that a future planar antenna array design is feasible. RF signal gain testing in a planar antenna arrangement with SMA switches is under investigation to create a working antenna array for multiband frequency applications.

ACKNOWLEDGMENTS

The authors would like to thank Dr. Karl Graff and Matt Short of Edison Welding Institute, Dr. John Volakis and Jing Zhao of the OSU Electro-Science Laboratory, and Ryan Hahnen of the Department of Mechanical and Aerospace Engineering. Financial support for this research was provided by the OSU Institute for Materials Research Interdisciplinary Materials Research Grant and the Smart Vehicle Concepts Center (www.SmartVehicleCenter.org), a National Science Foundation Industry/University Collaborative Research Center.

REFERENCES

- Caloz, C. 2009. “Perspectives on EM Metamaterials,” *Materials Today*, 12:12–20.
- Graff, K. 2005. *New Developments in Advanced Welding*, Woodhead Publishing Limited, Cambridge, UK.
- Hopkins, C.D., Fernandez, S.A. and Dapino, M.J. 2010. “Statistical Characterization of Ultrasonic Additive Manufacturing Ti/Al Composites,” *Journal of Engineering Materials and Technology*, 132:041006.
- Huang, W.M. 2002. “On the Selection of Shape Memory Alloys for Actuators,” *Materials and Design*, 23:11–19.
- Huang, W.M., Liu, Q.Y., He, L.M. and Yeo, J.H. 2004. “Micro NiTi–Si Cantilever With Three Stable Positions,” *Sensors and Actuators A*, 114:118–122.
- Janaki Ram, G.D., Yang, Y. and Stucker, B.E. 2006. “Effect of Process Parameters on Bond Formation During Ultrasonic Consolidation of Aluminum Alloy 3003,” *Journal of Manufacturing Systems*, 25:221.
- Johnson, K. 2008. “Interlaminar Subgrain Refinement in Ultrasonic Consolidation,” Ph.D. Thesis, Loughborough University, Loughborough, UK.
- Kong, C.Y. and Soar, R.C. 2005. “Fabrication of Metal–Matrix Composites and Adaptive Composites Using Ultrasonic Consolidation process,” *Materials Science & Engineering A*, 412:12–18.

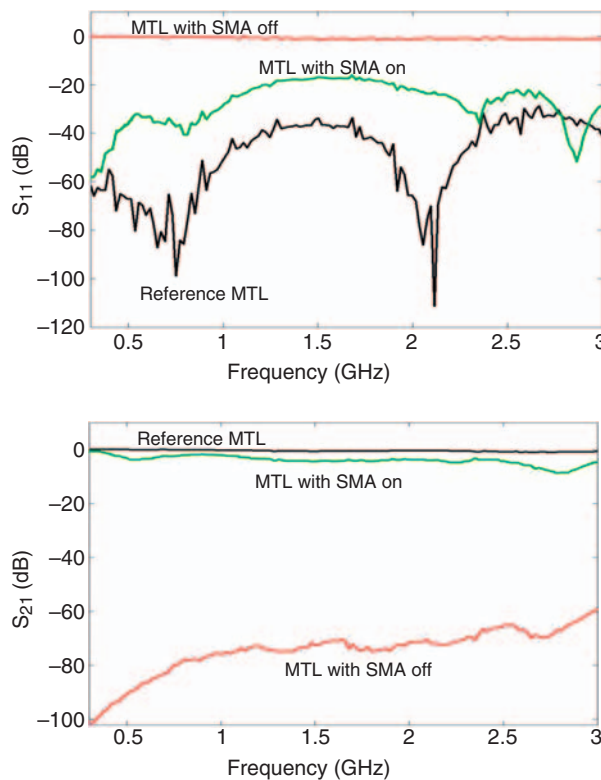


Figure 17. Signal performance of working MTL compared to reference with switch 2 on and off states.

- Kong, C.Y., Soar, R.C. and Dickens, P.M. 2004. "Optimum Process Parameters for Ultrasonic Consolidation of 3003 Aluminum," *Journal of Materials Processing Technology*, 146:181–187.
- Kraus, J. and Marhefka, R. 2003. *Antennas For All Applications*, 3rd edn, McGraw-Hill.
- Kulakov, M. and Rack, H.J. 2009. "Control of 3003-H18 Aluminum Ultrasonic Consolidation," *Journal of Engineering Materials and Technology*, 131:021006.
- Lagoudas, D. 2008. *Shape Memory Alloys*, Science and Business Media, LLC.
- Pozar, D. 2008. *Microwave Engineering*, 2nd edn, Science and Business Media, LLC.
- Siggard, E. 2007. "Investigative Research into the Structural Embedding of Electrical and Mechanical Systems using Ultrasonic Consolidation," MPhil Thesis, Utah State University, Logan, UT.
- The Aluminum Association. 1979. *Aluminum Standards and Data*, 6th edn, The Aluminum Association, Arlington, VA.
- Volakis, J., Mumcu, G., Sertel, K., Chen, C., Lee, M., Kramer, B., Psychoudakis, D. and Kiziltas, G. 2006. "Antenna Miniaturization Using Magnetic-Photonic and Degenerate Band-Edge Crystals," *IEEE Antennas and Propagation Magazine*, 48:12–28.
- Waram, T.C. 1993. *Actuator Design using Shape Memory Alloys*, Ontario Press, Canada.
- White, D.R. 2003. "Ultrasonic Consolidation of Aluminum Tooling," *Advanced Materials & Processes*, 161:64–65.
- Yashchyshyn, Y. 2010. "Reconfigurable Antennas: the State of the Art," *International Journal of Electronics and Telecommunications*, 56:319–326.
- Ziolkowski, R. 2008. "An Efficient, Electrically Small Antenna Designed for VHF and UHF Applications," *IEEE Antennas and Wireless Propagation Letters*, 7:217–220.